CMS Physics Analysis Summary

Contact: cms-pag-conveners-higgs@cern.ch 2012/11/14

Search for the standard model Higgs boson decaying to tau pairs

The CMS Collaboration

Abstract

A search for the standard model Higgs boson decaying to tau pairs is performed using events recorded by the CMS experiment at the LHC in 2011 and 2012 at a center-of-mass energy of 7 and 8 TeV respectively. The dataset corresponds to an integrated luminosity of 17 fb^{-1}, 4.9 fb^{-1} of data taken at 7 TeV center-of-mass energy and 12.1 fb^{-1} at 8 TeV. The tau-pair invariant-mass spectrum is studied in five different final states, $\mu\tau_h$+X, eτ_h+X, eμ+X, $\tau_h\tau_h$+X, and $\mu\mu$+X. Upper limits with respect to the standard model prediction in the mass range of 110-145 GeV are determined. An observed (expected) 95% confidence level exclusion limit for m_H = 125 GeV is found to be 1.63 (1.00) times the standard model cross section.

1 Introduction

An important goal of the LHC physics program is to ascertain the mechanism of electroweak symmetry breaking, through which the W and Z bosons attain mass. In the standard model (SM) [1–3], this is achieved via the Higgs mechanism [4–9], which also predicts the existence of a scalar Higgs boson. The Yukawa coupling of the Higgs field to fermions generates fermion masses. This aspect of the theory is tested directly in the search for Higgs bosons decaying to tau pairs.

On July 4, 2012, the discovery of a new boson, with mass around 125 GeV and with properties compatible with those of a standard-model Higgs boson, was announced at CERN by the ATLAS and CMS collaboration [10, 11]. The reported excess is most significant in the SM Higgs searches using the $\gamma\gamma$ and ZZ decay modes. The results for the $\tau\tau$ decay mode showed no excess of observed events in the mass range near 125 GeV, still compatible with a downward fluctuation from a background-only, and background plus SM Higgs hypothesis.

This Summary reports a search for the SM Higgs boson using final states with tau pairs in proton-proton collisions at $\sqrt{s} = 7$ and 8 TeV at the LHC. We use a data sample collected in 2011 and 2012 corresponding to an integrated luminosity of about 17 fb^{-1} recorded by the CMS [12] experiment, 4.9 fb^{-1} of data taken at 7 TeV center-of-mass energy and 12.1 fb^{-1} at 8 TeV.

Five independent tau pair final states are studied: $\mu\tau_h$+X, eτ_h+X, eμ+X, $\tau_h\tau_h$+X, and $\mu\mu$+X, where τ_h denotes a reconstructed hadronic decay of a tau.

In each channel, the signal is separated from the background, and in particular from the irreducible $Z \to \tau\tau$, using the tau-pair mass $m_{\tau\tau}$ reconstructed from the four momentum of the visible decay products of the two taus and from the $E_{\text{T}}^{\text{miss}}$, as explained in Section 4. Events are classified by the number of additional jets in the final state to enhance the contribution of different Higgs boson production mechanisms. The zero-jet categories are only used to constrain background normalizations, identification efficiencies, and energy scales. The one-jet categories select primarily signal events with a Higgs boson produced by gluon fusion, or in association with a W or Z boson decaying hadronically. These two categories are further classified according to the tau p_{T}, because high-p_{T} tau events benefit from a higher signal contribution and because these events typically feature a large $E_{\text{T}}^{\text{miss}}$ leading to an improved $m_{\tau\tau}$ resolution. Events in the vector-boson fusion (VBF) category are required to have two jets separated by a large rapidity gap, which mainly selects signal events with a Higgs boson produced by vector-boson fusion and strongly enhances the signal contribution.

The final result is combined with a Higgs search with tau pairs that uses the associated production of Higgs bosons with a W or Z boson decaying leptonically [13].

2 Event reconstruction

A particle-flow (PF) algorithm [14–16] combines the information from all CMS sub-detectors to identify and reconstruct the individual particles emerging from each collision event: charged hadrons, neutral hadrons, photons, muons, and electrons. These particles are then used to reconstruct the missing transverse energy $E_{\text{T}}^{\text{miss}}$, the jets, hadronic tau decays, and to quantify the lepton isolation.

In 2011 (2012), an average of 10 (20) proton-proton interactions occurred per LHC bunch crossing. Such a large number of interactions makes the identification of the vertex of the hard-

scattering process non-trivial, and affects most of the observables: jets, lepton isolation, etc. The tracking system is able to separate collision vertices as close as 0.5 mm. For each vertex, the sum of the p_{T}^2 of all tracks associated to the vertex is computed. The vertex for which this quantity is the largest is assumed to correspond to the hard-scattering process, and is referred to as the primary vertex.

Jets [17] are reconstructed from all the particles using the anti-k_T jet algorithm [18] implemented in FASTJET [19], with a distance parameter $D = 0.5$. The jet energy is corrected for the contribution of particles created in pile-up interactions and in the underlying event. This contribution is calculated as the product of the jet area and an event-by-event p_{T} density ρ, also obtained with FASTJET considering all particles in the event. Even though all particles are reconstructed by the PF algorithm at the right energy scale, a residual calibration factor is applied to the jet energy to account for imperfections in the neutral hadron calibration, the jet energy containment, and the estimation of the contribution of pile-up and underlying event particles. This factor, obtained from simulation, depends on the jet p_{T} and η, and is of the order of 5% across the whole acceptance. Finally, a percent level correction factor is applied to bring the jet energy response in the simulation to the one observed in the data. This correction factor and the jet energy scale uncertainty are extracted from a comparison between data and simulation in γ+jets, Z+jets, and di-jet events. Particles from pile-up vertices can be clustered into a pile-up jet, or seriously contaminate a jet from the primary vertex below the p_{T} threshold applied in the analysis. Such jets are identified and removed using a TMVA BDT [20] taking the following input variables: momentum and spatial distribution of the jet particles, charged and neutral particle multiplicities, compatibility of the jet charged hadrons with the primary vertex.

The resolution of the PF $E_{\mathrm{T}}^{\mathrm{miss}}$, reconstructed as the opposite of the vectorial sum of the transverse momenta of all particles, degrades rapidly with the number of pile-up interactions. In this analysis, a multivariate regression is used to provide a more precise measurement of the $E_{\mathrm{T}}^{\mathrm{miss}}$ in the presence of pile-up, the MVA PF $E_{\mathrm{T}}^{\mathrm{miss}}$. The regression is based on a TMVA BDT taking as input the PF $E_{\mathrm{T}}^{\mathrm{miss}}$ itself, as well as different flavors of the $E_{\mathrm{T}}^{\mathrm{miss}}$ computed with:

- charged hadrons from the primary vertex
- charged hadrons from the primary vertex, and neutral particles in jets passing the pile-up jet identification described above.
- charged hadrons from pile-up vertices and neutral particles in jets failing the pile-up jet identification.
- charged hadrons from the primary vertex and all neutral particles in the event. The vectorial sum of the transverse momenta of neutral particles within jets failing the pile-up jet identification is then added to this PF $E_{\mathrm{T}}^{\mathrm{miss}}$ flavor.

Figure 1 shows the resolution and response of the transverse recoil as a function of the number of reconstructed primary vertices, for the MVA and raw PF $E_{\mathrm{T}}^{\mathrm{miss}}$. For the average number of 20 primary vertices reconstructed in 2012, the resolution of the MVA PF $E_{\mathrm{T}}^{\mathrm{miss}}$ is a factor of two better than the one obtained with the traditional PF $E_{\mathrm{T}}^{\mathrm{miss}}$.

Jets originating from b-quark hadronization can be identified using a variety of algorithms exploiting their specific properties [21]. These properties, that result from the relatively large mass and long lifetime of b quarks, include the presence in the jets of tracks with large impact parameters, of secondary vertices displaced from the primary vertex, and of soft leptons from semi-leptonic b-hadron decays. The Combined Secondary Vertex (CSV) b-tagging algorithm combines the information about track impact parameters and secondary vertices in a likelihood discriminant to provide separation of b jets from jets originating from gluons, light quarks,

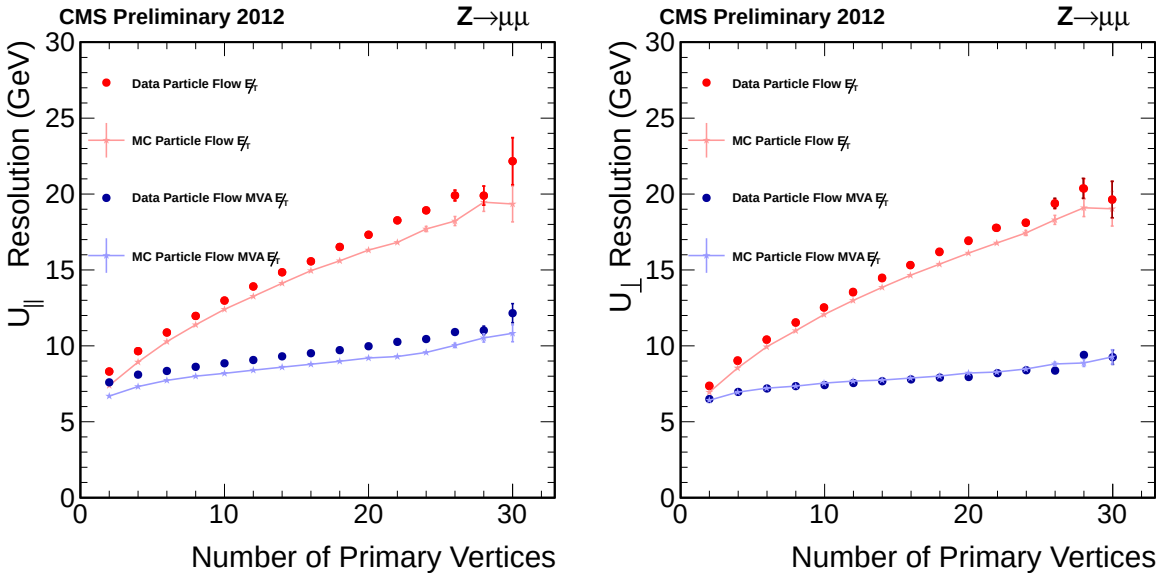

Figure 1: Resolution of the reconstructed recoil in Z boson events projected on the axis (left) parallel and (right) perpendicular to the direction of the Z boson momentum, versus the number of reconstructed primary vertices.

and charm quarks. The efficiency to tag b jets was measured using several techniques in the data and in the simulation using $t\bar{t}$ events and b-enriched multi-jet events. The latter were selected by requiring the presence in the event of a jet containing a muon, and identified as a b jet by both the soft-lepton and a reference lifetime-based identification algorithm. The other jets in the event are used to measure the efficiency of a separate identification algorithm. The probability to misidentify as b jet a jet originating from a non-b parton was determined from multijet events. A comparison between the data and the simulation was performed to obtain a correction factor for the b-tagging efficiency and the misidentification probability in the simulation as a function of the jet p_{T} and η, together with the systematic error on this correction factor.

Hadronically-decaying taus (τ_h) are reconstructed and identified using the so-called hadron-plus-strips algorithm [22], which targets the main decay modes by selecting candidates with one charged hadron and up to two neutral pions, or with three charged hadrons. The neutral pions are built by clustering the photons into strips along the ϕ direction to deal with possible photon conversions in the tracker material.

Taus from boson decay are typically isolated from the other particles in the event, in contrast to misidentified taus from jets which are surrounded by the jet particles not used in the tau reconstruction. The tau isolation R^{τ}_{Iso} is obtained from a multivariate discriminator taking in input a set of transverse momentum sums $S_j = \sum_i p_{\mathrm{T},i,j}$, where $p_{\mathrm{T},i,j}$ is the transverse momentum of a particle i in a ring j centered on the tau candidate and defined in the (η, ϕ) space. Five equal-width rings are used to cover up to a distance $\Delta R = \sqrt{\Delta\eta^2 + \Delta\phi^2} = 0.5$ from the tau candidate. The effect of pile-up on the isolation is mainly reduced by discarding the charged hadrons with a track originating from a pile-up vertex before the S_j calculation.

The isolation of electrons and muons is estimated relative to their transverse momentum p^{ℓ}_{T} as

$$R^{\ell}_{\mathrm{Iso}} \equiv \left(\sum_{\mathrm{charged}} p_{\mathrm{T}} + \mathrm{MAX}\left[0, \sum_{\mathrm{neutral}} p_{\mathrm{T}} + \sum_{\gamma} p_{\mathrm{T}} - 0.5 \sum_{\mathrm{charged,PU}} p_{\mathrm{T}} \right] \right) / p^{\ell}_{\mathrm{T}}, \qquad (1)$$

where $\sum_{\text{charged}} p_{\text{T}}$, $\sum_{\text{neutral}} p_{\text{T}}$, and $\sum_{\gamma} p_{\text{T}}$ are respectively the scalar sums of the transverse momenta of charged particles from the primary vertex, neutral hadrons, and photons located in a cone centered on the lepton direction in the (η, ϕ) space, of size $\Delta R = 0.4$. The contribution of pile-up photons and neutral hadrons is estimated from the scalar sum of the transverse momenta of charged hadrons from pile-up vertices in the cone, $\sum_{\text{charged,PU}} p_{\text{T}}$. This quantity is multiplied by 0.5, which corresponds approximately to the ratio of neutral to charged hadron production in the hadronization process of pile-up interactions.

3 Trigger and inclusive offline selection

The analysis makes use of the five independent tau-pair final states, $\mu\tau_h$+X, eτ_h+X, eμ+X, $\tau_h\tau_h$+X, and $\mu\mu$+X. In all five channels, the reducible and irreducible backgrounds are substantial.

The trigger selection requires a combination of electron, muon and tau trigger objects [23–25]. The particle-flow algorithm is used in the high-level trigger to reconstruct these objects and quantify their isolation as done in the offline reconstruction. The identification and isolation criteria and the transverse momentum thresholds for these objects were progressively tightened as the LHC instantaneous luminosity increased over the data-taking period. In the fully hadronic $\tau_h\tau_h$+X channel, the trigger fake rate is kept under control by requiring two relatively high transverse momentum tau trigger objects of $p_{\text{T}} > 30$ GeV, together with a jet trigger object of $p_{\text{T}} > 30$ GeV and $|\eta| < 3.1$, also reconstructed using the particle flow algorithm. This particular trigger was set up for the 2012 data taking period, making the $\tau_h\tau_h$+X analysis possible.

In the eτ_h+X, $\mu\tau_h$+X and $\tau_h\tau_h$+X channels, the leptons and τ_h are required to be loosely isolated in the trigger selection. This is not the case for the eμ+X and $\mu\mu$+X channels. For the eτ_h+X, $\mu\tau_h$+X and $\mu\mu$+X channels, the muon and electron triggering efficiencies were measured with respect to the offline selection in the data and in the simulation using Z events passing a single-lepton trigger. For the eμ+X channel, they were measured using $\text{Z} \to \tau\tau \to \text{e}\mu$ events passing a single-lepton trigger. The τ_h triggering efficiency was measured using $\text{Z} \to \tau\tau \to \mu\tau_h$ events passing a single-muon trigger. In the analysis, simulated events are weighted by the ratio between the efficiency measured in the data and the one measured in the simulation, which are parametrized as a function of the lepton or τ_h transverse momentum and pseudo-rapidity.

To be considered in the offline inclusive event selection, electrons and muons must fullfil tight isolation criteria and be isolated. Electrons and muons are required to have $R^{\ell}_{\text{Iso}} < 0.1$. The tau isolation discriminator R^{τ}_{Iso} defined in Section 2 is used to select isolated τ_h, in such a way that the overall tau identification efficiency amounts to 60-65%, for a jet fake rate of 2-3%. Finally, electrons and muons misidentified as τ_h are rejected using dedicated criteria based on the compatibility between the tracker, calorimeter, and muon chamber measurements.

In the eτ_h+X and $\mu\tau_h$+X channels, we select events containing an electron of $p_{\text{T}} > 20\,\text{GeV}$ or a muon of $p_{\text{T}} > 17\,\text{GeV}$, located within $|\eta| < 2.1$, and accompanied by an oppositely charged τ_h of $p_{\text{T}} > 20\,\text{GeV}$ within $|\eta| < 2.3$. In the 2012 dataset analysis, the electron and muon p_{T} thresholds have been increased to 24 GeV and 20 GeV, respectively, to account for higher trigger thresholds. In the eμ+X channel, we select events with an electron satisfying $|\eta| < 2.3$ and an oppositely charged muon within $|\eta| < 2.1$, requiring $p_{\text{T}} > 20\,\text{GeV}$ for the leading lepton and $p_{\text{T}} > 10\,\text{GeV}$ for the sub-leading lepton. In the $\tau_h\tau_h$+X channel, both τ_h are required to have $p_{\text{T}} > 45\,\text{GeV}$ and $|\eta| < 2.1$.

In the eτ_h+X and $\mu\tau_h$+X channels, events with more than one loosely identified electron or

muon with $p_T > 10\,\text{GeV}$ are rejected to reduce the Z$\rightarrow ll$ ($l = e, \mu$) background. The overlap between the various channels, including the ones of the associated production analysis described in Ref. [13], is eliminated by rejecting from the eτ_h+X ($\mu\tau_h$+X) channel events with an additional muon (electron), and by rejecting leptonic events from the $\tau_h\tau_h$+X channel.

Neutrinos produced in the tau decay are nearly collinear with the visible products, because the tau energy is much larger than its mass. Conversely, in W+jets events, one of the main backgrounds, the high mass of the W results in a neutrino approximately opposite to the lepton in the transverse plane, while a jet is misidentified as τ_h. In the eτ_h+X and $\mu\tau_h$+X channels, we therefore require the transverse mass

$$m_T = \sqrt{2 p_T E_T^{miss} (1 - \cos(\Delta\phi))} \tag{2}$$

to be less than 20 GeV, where p_T is the lepton transverse momentum and $\Delta\phi$ is the difference in ϕ between the lepton and the E_T^{miss} vector. In the eμ+X and the $\mu\mu$+X channels, we apply instead of a m_T requirement a cut $\not{p}_\zeta - 0.85 \cdot p_\zeta^{vis} > -20$ GeV, where

$$\not{p}_\zeta = \vec{E}_T^{miss} \cdot \vec{\zeta}, \tag{3}$$

$$p_\zeta^{vis} = \vec{p}_{T,1} \cdot \vec{\zeta} + \vec{p}_{T,2} \cdot \vec{\zeta}, \tag{4}$$

and where $\vec{\zeta}$ is a unit vector along the bisector of the directions of the leptons in the transverse plane [26], $\vec{p}_{T,i}$ are the lepton transverse momenta, and $\vec{E}_T^{miss}$ is the missing transverse energy vector, as illustrated in Fig. 2.

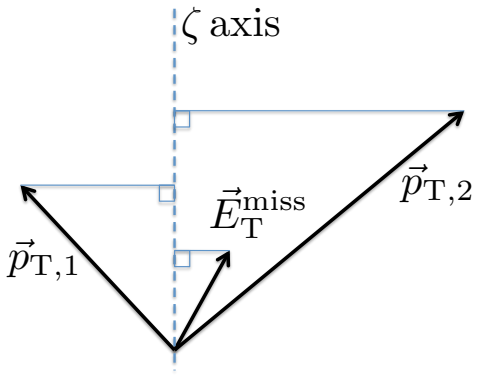

Figure 2: The ζ axis, and the projections onto this axis of the $\vec{E}_T^{miss}$ and of the transverse momenta $\vec{p}_{T,1}$ and $\vec{p}_{T,2}$ of the two leptons, shown in the transverse plane.

4 Tau-pair invariant mass reconstruction

The invariant mass m_{vis} of the visible decay products of the two taus can be used as an estimator of the mass of the parent boson, to separate the H $\rightarrow \tau\tau$ signal from the irreducible Z $\rightarrow \tau\tau$ background. A large amount of energy can however be transferred to the neutrinos produced in the tau decays, limiting the separation power of this estimator. Another possibility is to attempt a reconstruction of the neutrino energy using the collinear approximation [27], which has the disadvantage of providing an unphysical solution for about 20% of the events, in particular when the E_T^{miss} and the boson p_T are small. The SVFit algorithm presented in this Section reconstructs the mass $m_{\tau\tau}$ of the H and Z bosons with an improved resolution, and provides a physical solution for every event.

Six parameters are needed to specify tau decays to hadrons: the two decay angles in the tau rest frame, the three boost parameters to the laboratory frame, and the invariant mass of the visible decay products. In the case of a leptonic tau decay, two neutrinos are produced and the invariant mass of the di-neutrino system constitutes a seventh parameter. The unknown parameters are constrained by four observables which are the components of the four momentum of the system formed by the visible decay products of the tau, measured in the laboratory frame. For each hadronic (leptonic) tau decay, 2 (3) parameters are thus left unconstrained. We choose these parameters to be:

- x, the fraction of the tau energy in the laboratory frame carried by the visible decay products.
- ϕ, the azimuthal angle of the tau in the laboratory frame,
- $m_{\nu\nu}$, the mass of the neutrino system. In case of a hadronic tau decay, $m_{\nu\nu} \equiv 0$ GeV.

The two components E_x^{miss} and E_y^{miss} of the missing transverse energy vector provide two further constraints, albeit of a precision limited by the 10–15 GeV experimental resolution on these quantities [28, 29].

The fact that the reconstruction of tau pair decay kinematics is under-constrained by measured observables is addressed by a likelihood method. The mass $m_{\tau\tau}$ is reconstructed by combining the measured observables E_x^{miss} and E_y^{miss} with a probability model, which includes terms for tau decay kinematics and for the $E_{\text{T}}^{\text{miss}}$ resolution. The model makes a prediction for the probability density $p(\vec{z}|\vec{y},\vec{a_1},\vec{a_2})$ to observe the values $\vec{z} = (E_x^{\text{miss}}, E_y^{\text{miss}})$ measured in an event, given that the unknown parameters specifying the kinematics of the two tau decays have values $\vec{a_1} = (x_1, \phi_1, m_{\nu\nu,1})$ and $\vec{a_2} = (x_2, \phi_2, m_{\nu\nu,2})$, and that the 4-momenta of the visible decay products are equal to the measured values $\vec{y} = (p_1^{vis}, p_2^{vis})$. The likelihood model is used to compute the probability

$$P(m_{\tau\tau}^i) = \int \delta\left(m_{\tau\tau}^i - m_{\tau\tau}(\vec{y},\vec{a_1},\vec{a_2})\right) p(\vec{z}|\vec{y},\vec{a_1},\vec{a_2}) \mathrm{d}\vec{a_1} \mathrm{d}\vec{a_2}, \tag{5}$$

for a series of mass hypotheses $m_{\tau\tau}^i$. The best estimate $\hat{m}_{\tau\tau}$ for the mass $m_{\tau\tau}$ is taken to be the value of $m_{\tau\tau}^i$ maximizing $P(m_{\tau\tau}^i)$.

The probability density $p(\vec{z}|\vec{y},\vec{a_1},\vec{a_2})$ is the product of three likelihood functions, two of which model the decay kinematics $\vec{a_1}$ and $\vec{a_2}$ of the two taus, and the last one quantifies the compatibility of a tau decay hypothesis with the measured $E_{\text{T}}^{\text{miss}}$. The likelihood functions modeling the tau decay kinematics are different for leptonic and hadronic tau decays. Matrix elements taken from Ref. [30] are used to model the decays $\tau \to e\nu\nu$ and $\tau \to \mu\nu\nu$,

$$p_{\tau,l} = \frac{\mathrm{d}\Gamma}{\mathrm{d}x\mathrm{d}m_{\nu\nu}\mathrm{d}\phi} \propto \frac{m_{\nu\nu}}{4m_\tau^2}[(m_\tau^2 + 2m_{\nu\nu}^2)(m_\tau^2 - m_{\nu\nu}^2)], \tag{6}$$

within the physically allowed region $0 \leq x \leq 1$ and $0 \leq m_{\nu\nu} \leq m_\tau\sqrt{1-x}$. For decays of taus to hadrons, $\tau \to \tau_h\nu$, a model based on two–body phase space is used, treating all visible decay products of the tau as a single system,

$$p_{\tau,h} = \frac{\mathrm{d}\Gamma}{\mathrm{d}x\mathrm{d}\phi} \propto \frac{1}{1 - \frac{m_{vis}^2}{m_\tau^2}}, \tag{7}$$

within the physically allowed region $\frac{m_{vis}^2}{m_\tau^2} \leq x \leq 1$. We have verified that the two–body phase space model is adequate for representing hadronic tau decays by comparing distributions of

the visible energy fraction x in tau decays generated by a toy Monte Carlo based on the two–body phase space model with the detailed simulation of hadronic tau decays implemented in TAUOLA. The likelihood functions for leptonic (hadronic) tau decays do not depend on the parameters x and ϕ (x, ϕ and $m_{\nu\nu}$). The dependence on x enters via the integration boundaries, and the dependence on ϕ comes from the $E_{\mathrm{T}}^{\mathrm{miss}}$ likelihood.

The $E_{\mathrm{T}}^{\mathrm{miss}}$ likelihood p_{MET} quantifies the compatibility of a tau decay hypothesis with the missing transverse momentum reconstructed in an event, assuming the neutrinos produced in tau decays to be the only source of $E_{\mathrm{T}}^{\mathrm{miss}}$, and is defined as

$$p_{\mathrm{MET}}(E_x^{\mathrm{miss}}, E_y^{\mathrm{miss}}) = \frac{1}{2\pi\sqrt{|V|}} \cdot \exp\left(-\frac{1}{2} \begin{pmatrix} E_x^{\mathrm{miss}} - \sum p_x^{\nu} \\ E_y^{\mathrm{miss}} - \sum p_y^{\nu} \end{pmatrix}^T \cdot V^{-1} \cdot \begin{pmatrix} E_x^{\mathrm{miss}} - \sum p_x^{\nu} \\ E_y^{\mathrm{miss}} - \sum p_y^{\nu} \end{pmatrix} \right). \quad (8)$$

In this expression, the expected resolution of the $E_{\mathrm{T}}^{\mathrm{miss}}$ reconstruction is represented by the covariance matrix V estimated on an event–by–event basis using the $E_{\mathrm{T}}^{\mathrm{miss}}$–significance algorithm [31], and $|V|$ is the determinant of this matrix.

The resolution achieved by the SVFit algorithm in reconstructing $m_{\tau\tau}$ typically amounts to 20% of the true $m_{\tau\tau}$. Figure 3 shows a clear separation between the $m_{\tau\tau}$ distributions obtained for the $Z \to \tau\tau$ background and for a SM Higgs boson signal sample with $m_H = 125$ GeV.

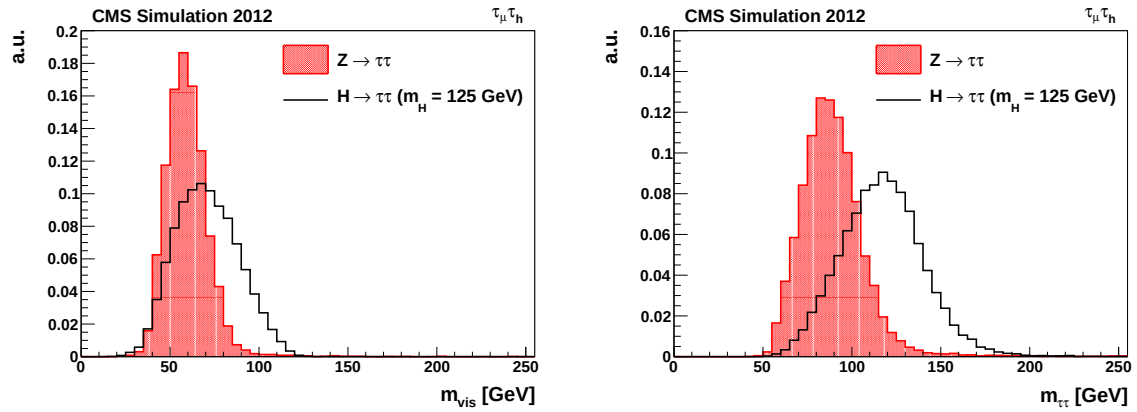

(a) (b)

Figure 3: Simulated visible mass m_{vis} (left) and SVFit mass $m_{\tau\tau}$ (right) normalized distributions obtained in the $\mu\tau_h$+X channel after the inclusive selection for the $Z \to \tau\tau$ background and a SM Higgs boson signal sample with $m_H = 125$ GeV.

5 Exclusive event categories

To further enhance the sensitivity of the search for Higgs bosons, the selected events are split into mutually exclusive categories based on the jet multiplicity, and on the transverse momentum of the reconstructed tau decay products. The jet event categories are defined in the following way for the leptonic channels, using jets within $|\eta| < 4.7$.

- **VBF:** In this category, two jets with $p_{\mathrm{T}} > 30$ GeV are required to tag the vector-boson fusion Higgs production process. The two jets must have an invariant mass $M_{jj} > 500$ GeV and be separated in pseudo-rapidity by $\Delta\eta > 3.5$. A rapidity gap is defined by requiring no reconstructed jet with $p_{\mathrm{T}} > 30$ GeV between the two

tagging jets. In the eμ+X channel, the large $\mathrm{t\bar{t}}$ background contribution is suppressed by rejecting events with a b-tagged jet with $p_{\mathrm{T}} > 20$ GeV.

- **1-Jet:** Events in this category are required to have at least one jet with $p_{\mathrm{T}} > 30$ GeV, not to be part of the VBF event category, and not to contain any b-tagged jet with $p_{\mathrm{T}} > 20$ GeV. This category exploits the production of a high-p_{T} Higgs boson recoiling against a jet. Events with high-p_{T} Higgs bosons typically have much larger $E_{\mathrm{T}}^{\mathrm{miss}}$ and benefit from an improved resolution on $E_{\mathrm{T}}^{\mathrm{miss}}$, and thus on $m_{\tau\tau}$. In addition, τ pairs produced in the Drell-Yan process are expected to have a softer p_{T} spectrum. In the eτ_h+X channel, the large background from $\mathrm{Z}\rightarrow ee$ + jets events in which an electron is misidentified as τ_h is reduced by requiring $E_{\mathrm{T}}^{\mathrm{miss}} > 30$ GeV.
- **0-Jet:** This category contains all events with no jet with $p_{\mathrm{T}} > 30$ GeV, and no b-tagged jet with $p_{\mathrm{T}} > 20$ GeV. The 0-Jet categories are only used to constrain background normalizations, identification efficiencies, and energy scales.

The 1-Jet and 0-Jet categories are split in two bins of reconstructed tau p_{T}. In the eτ_h+X and $\mu\tau_h$+X channels the threshold is at $p_{\mathrm{T}} > 40$ GeV of the τ_h, while the threshold is 35 GeV on the muon in the eμ+X channel and 30 GeV on the leading muon in the $\mu\mu$+X channel.

In the $\tau_h\tau_h$+X channel, a leading jet with $p_{\mathrm{T}} > 50$ GeV and $|\eta| < 2.1$ is required to match the trigger requirement, and two categories are defined:

- **VBF**: A sub-leading jet with $p_{\mathrm{T}} > 30$ GeV must be present. The two-jet system must have $M_{jj} > 250$ GeV and be separated by a pseudo-rapidity gap of $\Delta\eta > 2.5$ with no other jet with $p_{\mathrm{T}} > 30$ GeV. The multijet background is reduced by asking $p_{\mathrm{T,H}} > 110$ GeV.
- **1-Jet:** In this category, the transverse momentum $p_{\mathrm{T,H}}$ of the system formed by the two τ_h and the $E_{\mathrm{T}}^{\mathrm{miss}}$ is required to be greater than 140 GeV, to reduce the multijet background.

5.1 Comparison with previous results

The sensitivity of the new analysis has improved due to additional data and the revised $E_{\mathrm{T}}^{\mathrm{miss}}$ reconstruction with respect to the results reported in [11]. The improved $E_{\mathrm{T}}^{\mathrm{miss}}$ resolution translates into a superior di-τ mass resolution that allows better separation of signal and background events. The selection of VBF events has been simplified, while keeping similar sensitivity to the SM Higgs. The working point for the VBF selection, transverse mass and missing transverse energy requirements have been optimized. The resulting working point of the selection in the VBF categories has higher purity. The overlap of events used in the $\mu\tau_h$+X channel in the previous analysis in the same dataset is rather small.

In this version of the analysis, the 0-Jet categories are not used to fit for the signal strength. Additional studies are necessary to reduce and constrain the challenging $\mathrm{Z}\rightarrow \ell\ell$ (ℓ =e, μ) background, where an electron or muon is misidentified as an hadronic tau decay. This background is of particular importance in the 0-Jet and high-p_{T} categories where the fit for signal is not well constrained due to the similar shape of signal and background. The expected performance of the overall Higgs search is degraded by 5 %. We verified that a possible signal has negligible impact on the constrained nuisances.

6 Background estimation

The observed number of events for each category, as well as the expected number of events from various background processes, are shown in Tables 2–5 together with expected signal yields and efficiencies. The background yields are input to a fit for the signal discussed in Section 8

The largest source of events selected with these requirements is $Z \to \tau\tau$ decays. We estimate the contribution from this process using an observed sample of $Z \to \mu\mu$ events, where the reconstructed muons are replaced by the reconstructed particles from simulated tau decays, a procedure called *embedding*. The normalization for this process is determined from the measurement of the $Z \to \mu\mu$ yield in data.

Another significant source of background is multijet events in which there is one jet misidentified as an isolated electron or muon, and a second jet misidentified as τ_h. W+jets events in which there is a jet misidentified as a τ_h are also a source of background. The rates for these processes are estimated using the number of observed same-charge tau pair events, and from events with large transverse mass, respectively. For the $\tau_h\tau_h$+X channel, the shape of the multijet background is estimated from events with opposite-sign charge where the isolation requirement on one of the two taus satisfies a relaxed criterion but does not satisfy the full isolation criterion. The contributions from non-multijet backgrounds are estimated from simulation and subtracted. The yield of the multijet contribution in the opposite-charge (OC) signal region is estimated by scaling OC events where the isolation on one the candidate is relaxed. The scale factor is measured using corresponding selections in events where the candidates have the same charge.

Other background processes include $t\bar{t}$ production and $Z \to ee/\mu\mu$ events, particularly in the $e\tau_h$+X channel due to the 2–3% probability for electrons to be misidentified as τ_h [22]. The small background from W+jets and multijet events for the $e\mu$+X channel where jets are misidentified as isolated leptons is derived by measuring the number of events with one good lepton and a second one which passes relaxed selection criteria, but fails the nominal lepton selection. This sample is extrapolated to the signal region using the efficiencies for such loose lepton candidates to pass the nominal lepton selection. These efficiencies are measured in data using multijet events. Backgrounds from $t\bar{t}$ and di-boson production are estimated from simulation using the MADGRAPH [32] event generator to simulate the shapes for $t\bar{t}$ events, and PYTHIA 6.424 [33] to simulate the shapes for di-boson events. The event yields are determined from measurements in background-enriched sideband regions.

To model the SM Higgs boson signals the event generators PYTHIA and POWHEG [34] are used. The TAUOLA [35] package is used for tau decays in all cases. Additional next-to-next-to-leading order (NNLO) K-factors from FEHIPRO [36, 37] are applied to the Higgs boson p_T spectrum from Higgs boson events produced via gluon fusion for samples produced at $\sqrt{s}$ = 7 TeV. Samples produced at $\sqrt{s}$ = 8 TeV use an improved version of POWHEG which shows good agreement in the Higgs boson p_T spectrum at NNLO.

The presence of pile-up is incorporated by simulating additional interactions and then reweighting the simulated events to match the distribution of additional interactions observed in data. The events in the embedded $Z \to \tau\tau$ sample and in other background samples obtained from data contain the correct distribution of pile-up interactions. The missing transverse energy response from simulation is corrected using a prescription, based on data, developed for inclusive W and Z cross section measurements [38], where Z bosons are reconstructed in the dimuon channel, and the missing transverse energy scale and resolution calibrated as a function of the

Z boson transverse momentum.

Table 1: Numbers of expected and observed events in the event categories for the data taken in 2011 and 2012 as described in the text for the $\mu\tau_h$+X channel. Categories of high and low tau p_T are summed. Also given are the expected signal yields and the reconstruction and selection efficiency for a SM Higgs boson with $m_H = 125$ GeV in the various production channels considered. Combined statistical and systematic uncertainties on each estimate are reported.

Process	*0-Jet*	*1-Jet*	*VBF*
Z$\to \tau\tau$	64948 $\pm$ 3628	13292 $\pm$ 745	80 $\pm$ 9
QCD	12515 $\pm$ 622	3156 $\pm$ 222	32 $\pm$ 5
W+jets	5160 $\pm$ 615	3610 $\pm$ 233	36 $\pm$ 3
Z+jets (l/jet faking τ)	1200 $\pm$ 193	452 $\pm$ 52	1 $\pm$ 0.4
$t\bar{t}$	8 $\pm$ 0.8	350 $\pm$ 34	4 $\pm$ 1
Dibosons	95 $\pm$ 10	216 $\pm$ 25	1 $\pm$ 0.4
Total Background	83926 $\pm$ 3736	21076 $\pm$ 815	154 $\pm$ 10
H$\to \tau\tau$	-	112 $\pm$ 9	8 $\pm$ 0.9
Data	81297	21107	174
Signal Eff.			
gg$\to$ H	-	$4.50 \cdot 10^{-3}$	$8.41 \cdot 10^{-5}$
qq$\to$ H	-	$9.75 \cdot 10^{-3}$	$3.90 \cdot 10^{-3}$
qq$\to$ H$t\bar{t}$ or VH	-	$6.19 \cdot 10^{-3}$	$1.52 \cdot 10^{-5}$

Table 2: Numbers of expected and observed events in the event categories for the data taken in 2011 and 2012 as described in the text for the eτ_h+X channel. Categories of high and low tau p_T are summed. Also given are the expected signal yields and the reconstruction and selection efficiencies for a SM Higgs boson with $m_H = 125$ GeV in the various production channels considered. Combined statistical and systematic uncertainties on each estimate are reported.

Process	*0-Jet*	*1-Jet*	*VBF*
Z$\to \tau\tau$	19127 $\pm$ 1010	2042 $\pm$ 111	34 $\pm$ 4
QCD	6178 $\pm$ 411	149 $\pm$ 11	16 $\pm$ 4
W+jets	1967 $\pm$ 224	711 $\pm$ 44	20 $\pm$ 2
Z+jets (l/jet faking τ)	4445 $\pm$ 527	50 $\pm$ 7	8 $\pm$ 1
$t\bar{t}$	3 $\pm$ 0.4	96 $\pm$ 8	3 $\pm$ 0.9
Dibosons	30 $\pm$ 3	49 $\pm$ 5	1 $\pm$ 1
Total Background	31750 $\pm$ 1232	3097 $\pm$ 121	82 $\pm$ 6
H$\to \tau\tau$	-	28 $\pm$ 2	4 $\pm$ 0.4
Data	31646	2985	80
Signal Eff.			
gg$\to$ H	-	$1.03 \cdot 10^{-3}$	$3.44 \cdot 10^{-5}$
qq$\to$ H	-	$2.89 \cdot 10^{-3}$	$1.93 \cdot 10^{-3}$
qq$\to$ H$t\bar{t}$ or VH	-	$1.93 \cdot 10^{-3}$	$2.22 \cdot 10^{-6}$

Table 3: Numbers of expected and observed events in the event categories for the data taken in 2011 and 2012 as described in the text for the eμ+X channel. Categories of high and low tau p_{T} are summed. Also given are the expected signal yields and the reconstruction and selection efficiencies for a SM Higgs boson with $m_H = 125$ GeV in the various production channels considered. Combined statistical and systematic uncertainties on each estimate are reported.

Process	*0-Jet*	*1-Jet*	*VBF*
Z$\rightarrow \tau\tau$	34371 $\pm$ 1171	8118 $\pm$ 329	43 $\pm$ 4
QCD	2142 $\pm$ 485	894 $\pm$ 192	8 $\pm$ 2
$t\bar{t}$	45 $\pm$ 3	1498 $\pm$ 113	15 $\pm$ 3
Dibosons	929 $\pm$ 83	785 $\pm$ 76	6 $\pm$ 1
Total Background	37487 $\pm$ 1270	11295 $\pm$ 404	73 $\pm$ 5
H$\rightarrow \tau\tau$	-	58 $\pm$ 5	4 $\pm$ 0.4
Data	38345	11161	80
Signal Eff.			
gg$\rightarrow$ H	-	$2.29 \cdot 10^{-3}$	$3.43 \cdot 10^{-5}$
qq$\rightarrow$ H	-	$4.93 \cdot 10^{-3}$	$1.98 \cdot 10^{-3}$
qq$\rightarrow$ H$t\bar{t}$ or VH	-	$3.88 \cdot 10^{-3}$	$1.42 \cdot 10^{-5}$

Table 4: Numbers of expected and observed events in the event categories for the data taken in 2011 and 2012 as described in the text for the $\tau_h\tau_h$+X channel. Categories of high and low tau p_{T} are summed. Also given are the expected signal yields and the reconstruction and selection efficiencies for a SM Higgs boson with $m_H = 125$ GeV in the various production channels considered. Combined statistical and systematic uncertainties on each estimate are reported.

Process	*1-Jet*	*VBF*
Z$\rightarrow \tau\tau$	281 $\pm$ 56	18 $\pm$ 4
QCD	109 $\pm$ 33	28 $\pm$ 8
W+jets	53 $\pm$ 16	13 $\pm$ 4
Z+jets (l/jet faking τ)	5 $\pm$ 1	0.0 $\pm$ 0.0
$t\bar{t}$	48 $\pm$ 11	2 $\pm$ 0.6
Dibosons	5 $\pm$ 1	0.0 $\pm$ 0.0
Total Background	503 $\pm$ 67	61 $\pm$ 10
H$\rightarrow \tau\tau$	6 $\pm$ 1	2 $\pm$ 0.3
Data	511	66
Signal Eff.		
gg$\rightarrow$ H	$2.44 \cdot 10^{-4}$	$4.16 \cdot 10^{-5}$
qq$\rightarrow$ H	$5.07 \cdot 10^{-4}$	$8.11 \cdot 10^{-4}$
qq$\rightarrow$ H$t\bar{t}$ or VH	$1.38 \cdot 10^{-3}$	$3.12 \cdot 10^{-5}$

Table 5: Numbers of expected and observed events in the event categories for the data taken in 2011 and 2012 as described in the text for the $\mu\mu$+X channel. Categories of high and low tau p_{T} are summed. Also given are the expected signal yields and the reconstruction and selection efficiencies for a SM Higgs boson with $m_H = 125$ GeV in the various production channels considered. Combined statistical and systematic uncertainties on each estimate are reported.

Process	*0-Jet*	*1-Jet*	*VBF*
Z$\to \tau\tau$	15202 $\pm$ 519	4047 $\pm$ 169	87 $\pm$ 8
QCD	1026 $\pm$ 50	520 $\pm$ 34	7 $\pm$ 4
W+jets	85 $\pm$ 10	36 $\pm$ 6	0.0 $\pm$ 0.0
Z$\to \mu\mu$	1425917 $\pm$ 87705	530352 $\pm$ 39352	256 $\pm$ 54
$t\bar{t}$	3996 $\pm$ 361	1942 $\pm$ 184	16 $\pm$ 3
Dibosons	2479 $\pm$ 581	4587 $\pm$ 1118	11 $\pm$ 4
Total Background	1448705 $\pm$ 87710	541484 $\pm$ 39368	377 $\pm$ 56
H$\to \tau\tau$	-	36 $\pm$ 3	3 $\pm$ 0.6
Data	1420083	533257	360
Signal Eff.			
gg$\to$ H	-	$1.39 \cdot 10^{-3}$	$6.99 \cdot 10^{-5}$
qq$\to$ H	-	$2.93 \cdot 10^{-3}$	$1.17 \cdot 10^{-3}$
qq$\to$ H$t\bar{t}$ or VH	-	$3.64 \cdot 10^{-3}$	$1.65 \cdot 10^{-4}$

7 Systematic uncertainties

Various imperfectly known or simulated effects can alter the shape and normalization of the invariant mass spectrum. The main contributions to the normalization uncertainty include the uncertainty in the total integrated luminosity, 2.2% in 7 TeV and 4.5% in 8 TeV data [39], jet energy scale (2–5% depending on η and p_{T}), background normalization (Tables 2– 5), Z boson production cross section (2.5%) [38], lepton identification and isolation efficiency (1.0%), and trigger efficiency (1.0%). The tau-identification efficiency uncertainty is estimated to be 8% from an independent study done using a tag-and-probe technique [38] including the uncertainty of the trigger efficiency. The lepton identification and isolation efficiencies are stable as a function of the number of additional interactions in the bunch crossing in data and in Monte Carlo simulation, and are measured to 2% precision. The b-tagging efficiency carries an uncertainty of about 5%, and the b-mistag rate is accurate to about 10% [40]. Uncertainties that contribute to mass spectrum shape variations include the tau (3%), muon (1%), and electron (1.5%) energy scales. The effect of the uncertainty on the $E_{\mathrm{T}}^{\mathrm{miss}}$ scale, mainly due to pile-up effects, is incorporated by varying the mass spectrum shape as described in the next section.

The various production cross sections and branching fractions for SM and corresponding uncertainties are taken from [41–65]. Theoretical uncertainties on the Higgs production cross section are included in the statistical interpretation. These uncertainties are 12% for gluon fusion and 10% for VBF production.

8 Maximum likelihood fit

To search for the presence of a Higgs boson signal in the selected events, we perform a binned maximum likelihood fit to the tau-pair invariant-mass spectrum. The fit is performed jointly across the five final states with two or five event categories each.

Systematic uncertainties are represented by nuisance parameters in the fitting process. We assume log-normal priors for normalization parameters, and Gaussian priors for mass-spectrum shape uncertainties. The uncertainties that affect the shape of the mass spectrum, mainly those corresponding to the energy scales, are represented by nuisance parameters whose variation results in a continuous perturbation of the spectrum shape [66].

9 Results

Figures 5 to 8 show the distributions of $m_{\tau\tau}$ for each event category compared with the background prediction. The categories of different tau-p_{T} are summed for the 0-Jet category.

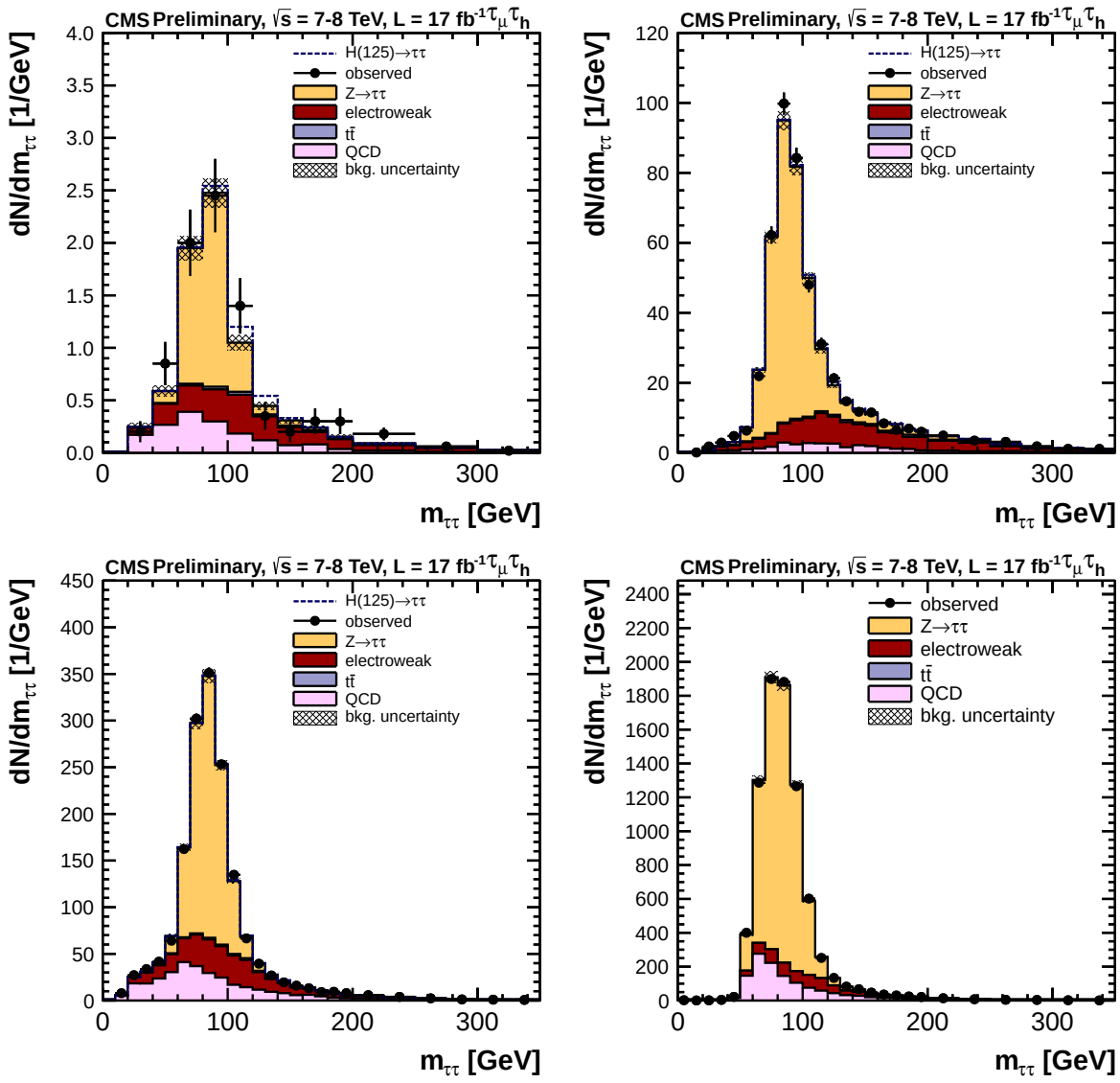

Figure 4: Distribution of the tau-pair invariant mass for the $\mu\tau_h$+X channel in the SM Higgs boson search categories: VBF category (top left), 1-Jet high tau p_{T} category (top right), 1-Jet low tau p_{T} category (bottom left), and 0-Jet category (bottom right). The background labelled 'electroweak' combines the contribution from W+jets, Z$\to \ell\ell$, and diboson processes.

The invariant mass spectra show no evidence for the presence of a Higgs boson signal, and we

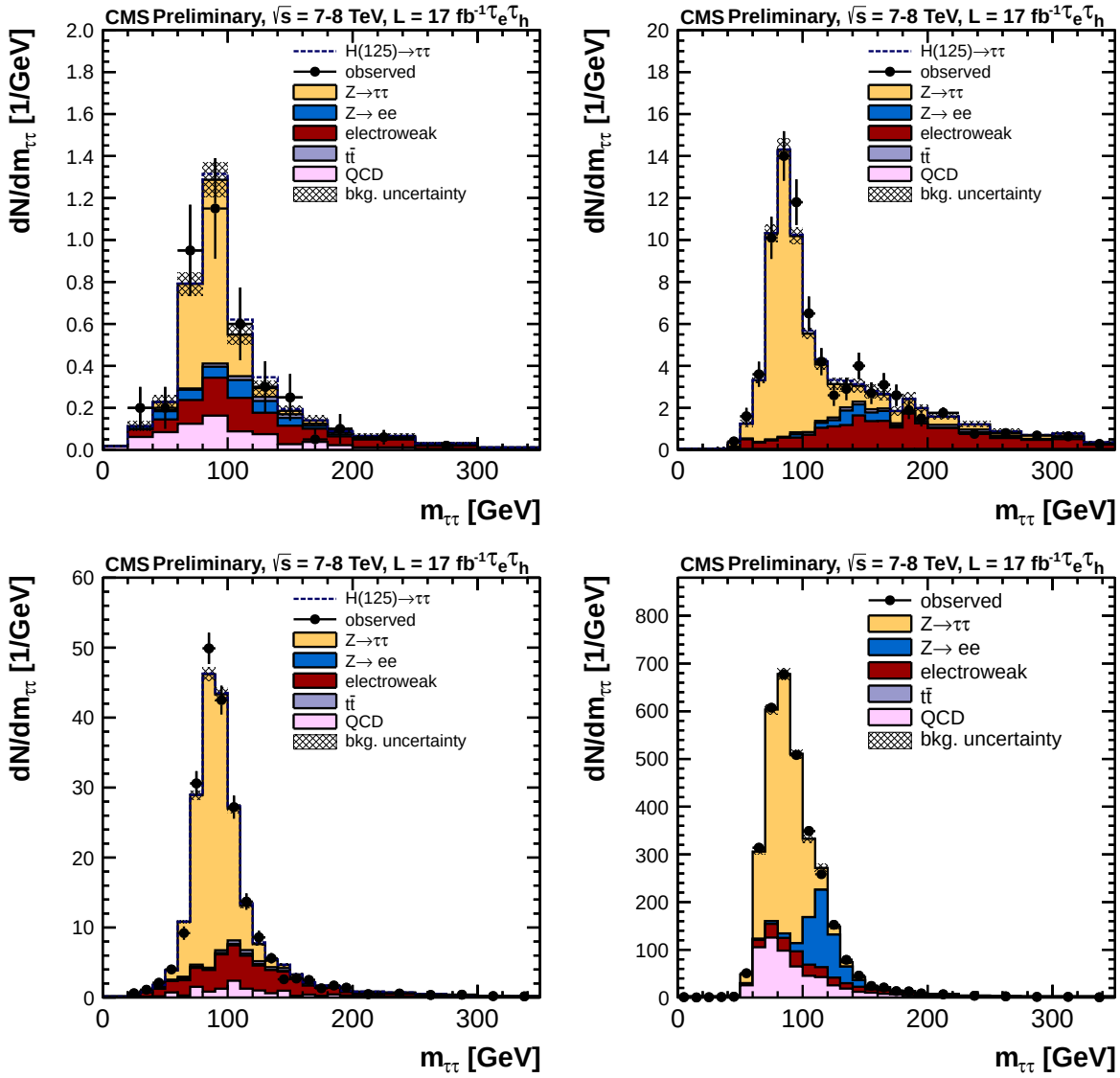

Figure 5: Distribution of the tau-pair invariant mass for the eτ_h+X channel in the SM Higgs boson search categories: VBF category (top left), 1-Jet high tau p_{T} category (top right), 1-Jet low tau p_{T} category (bottom left), and 0-Jet category (bottom right). The background labelled 'electroweak' combines the contribution from W+jets, Z$\rightarrow$ ll, and diboson processes.

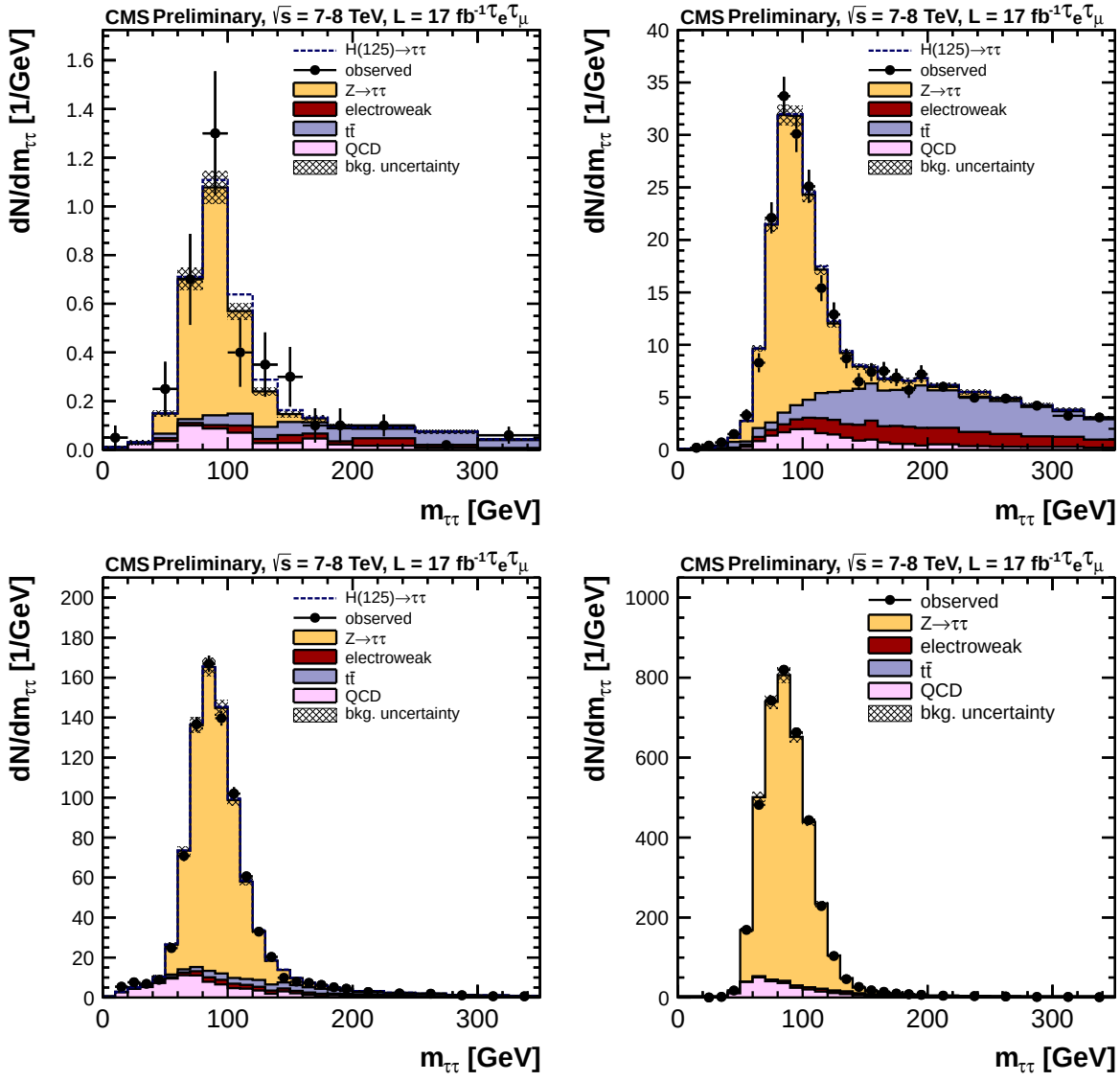

Figure 6: Distribution of the tau-pair invariant mass for the eμ+X channel in the SM Higgs boson search categories: VBF category (top left), 1-Jet high tau p_{T} category (top right), 1-Jet low tau p_{T} category (bottom left), and 0-Jet category (bottom right).

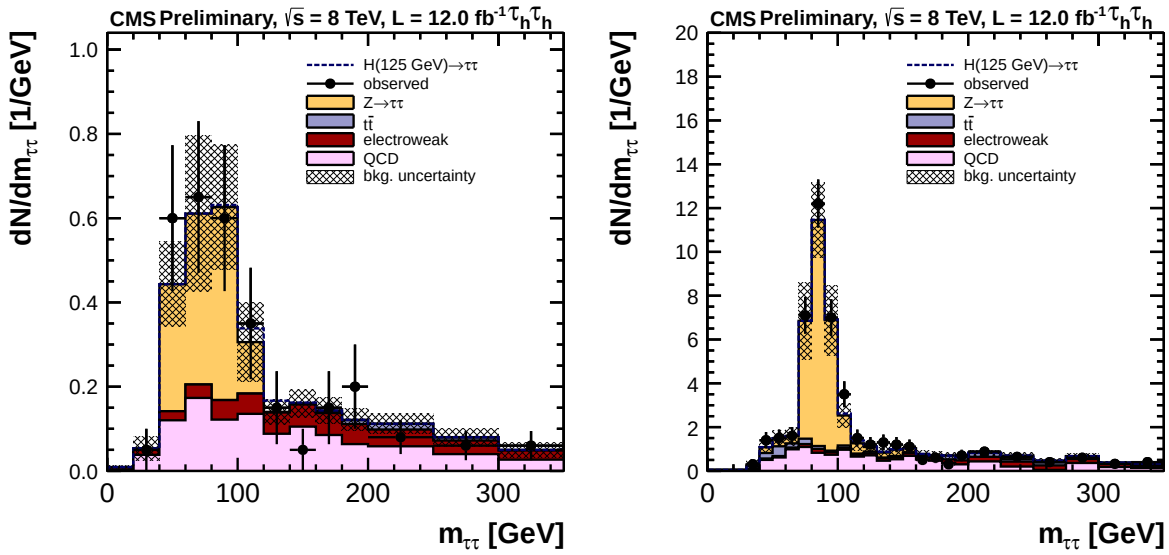

Figure 7: Distribution of the tau-pair invariant mass for the $\tau_t\tau_h$+X channel in the SM Higgs boson search categories: VBF category (top left), and 1-Jet category (top right). The background labelled 'electroweak' combines the contribution from W+jets, Z$\to ll$, and diboson processes.

therefore set 95% confidence level (CL) upper bounds on the Higgs boson cross section times the branching fraction into a tau pair. For calculations of exclusion limits, we use the modified frequentist construction CL$_s$ [67–69]. Theoretical uncertainties on the Higgs boson production cross sections are taken into account as systematic uncertainties in the limit calculations.

9.1 Limits on SM Higgs boson production

The 1-Jet and VBF categories are used to set a 95% CL upper limit on the product of the Higgs boson production cross section and the H $\to \tau\tau$ branching fraction, $\sigma_{\mathrm{H}} \times \mathrm{BR}(\mathrm{H} \to \tau\tau)$, with respect to the SM Higgs expectation, $\sigma/\sigma_{\mathrm{SM}}$. Figure 9 shows the observed and the mean expected 95% CL upper limits for Higgs boson mass hypotheses ranging from 110 to 145 GeV. The bands represent the one- and two-standard-deviation probability intervals around the expected limit. Table 6 summarizes the observed and expected limits and Table 7 shows the significance for the combination of all tau-pair search channels as a function of the Higgs mass hypothesis.

9.2 Signal strength in combination and sub-combinations

The total signal strength, $\sigma/\sigma_{\mathrm{SM\,H}}$, is measured to 0.7$\pm$0.5 at m_{H} = 125 GeV. Figure 10 shows the compatibility of individual Higgs production and di-tau decay modes. These compatibility tests do not constitute measurements of any physics parameters per se, but rather show the consistency of the various observations with the expectations for the SM Higgs boson. The estimation of the signal strength in sub-combinations does not utilize constraints of nuisances from categories not included in the fit.

10 Summary

We have reported a search for the SM Higgs boson, using a sample of CMS data from proton-proton collisions at a center-of-mass energy of 7 and 8 TeV at the LHC, corresponding to an integrated luminosity of 17 fb^{-1}. The tau-pair events are studied in five different final states,

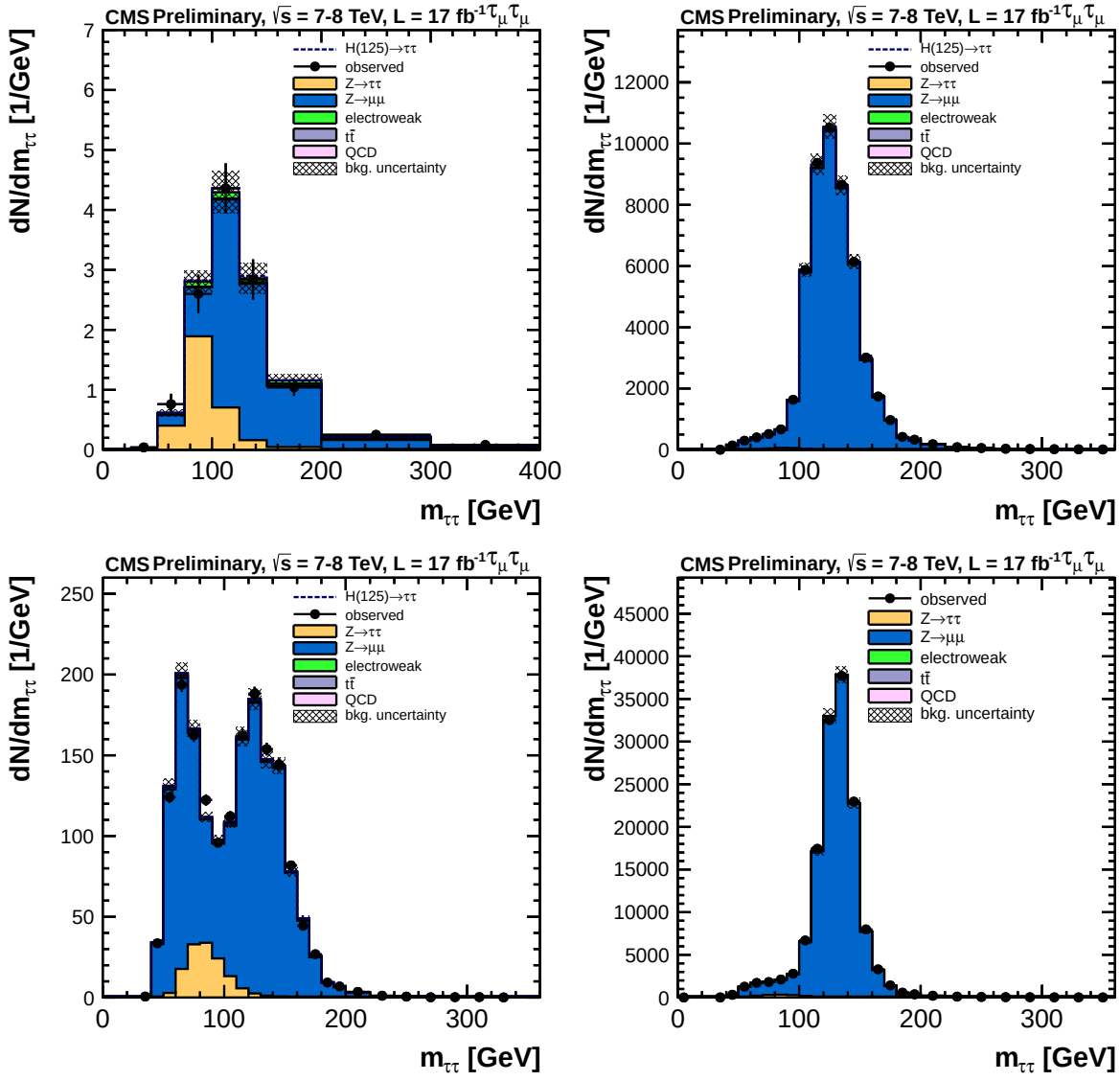

Figure 8: Distribution of the tau-pair invariant mass for the $\mu\mu$+X channel in the SM Higgs boson search categories: VBF category (top left), 1-Jet high tau p_{T} category (top right), 1-Jet low tau p_{T} category (bottom left), and 0-Jet category (bottom right).

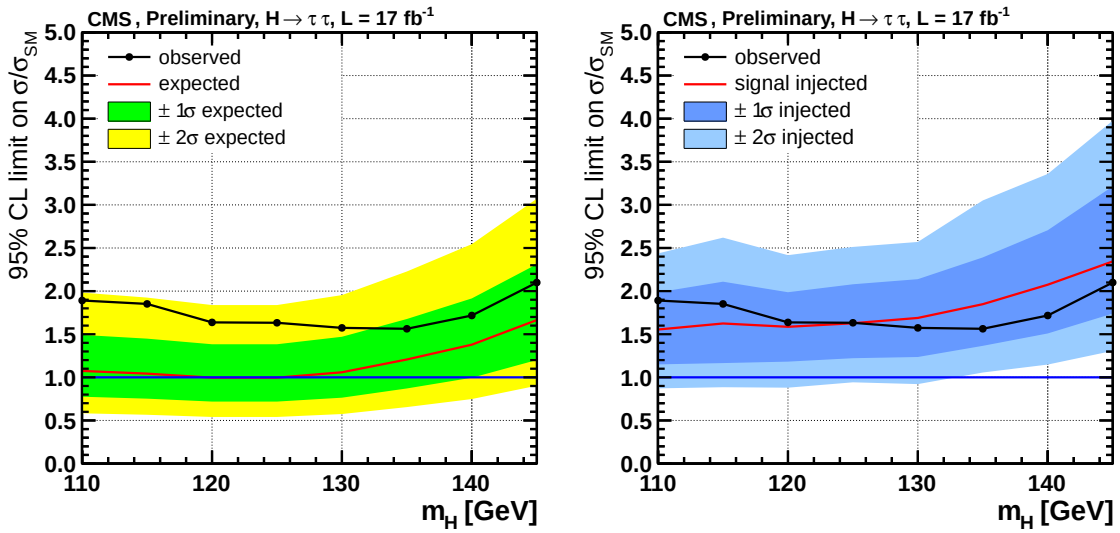

Figure 9: The observed 95% CL upper limit is shown together with the expected one- and two-standard-deviation ranges on the cross section, normalized to the SM expectation for Higgs boson production, as a function of m_{H}. The plot on the left shows the expected and observed result for the background-only hypothesis, while the plot on the right includes a standard-model Higgs boson with $m_{\mathrm{H}} = 125$ GeV for the expected result. The observed result is identical in both figures. The combined Higgs to tau-pair result includes a dedicated search using the associated production mechanism.

Table 6: Observed 95% CL upper limits on the cross section, divided by the expected SM Higgs cross section as a function of m_{H} together with the expected range. The combined Higgs to tau-pair result includes a dedicted search using the associated production mechanism.

SM Higgs	Expected limit					
m_{H} [GeV]	-2σ	-1σ	Median	$+1\sigma$	$+2\sigma$	Obs. Limit
110	0.58	0.78	1.07	1.49	1.98	1.89
115	0.57	0.75	1.04	1.45	1.92	1.85
120	0.54	0.72	1.00	1.38	1.84	1.64
125	0.54	0.72	1.00	1.38	1.84	1.63
130	0.57	0.76	1.06	1.47	1.95	1.57
135	0.65	0.87	1.21	1.68	2.23	1.56
140	0.75	1.00	1.38	1.92	2.54	1.72
145	0.90	1.20	1.66	2.31	3.07	2.10

Table 7: Expected and observed significance as a function of m_{H}. The combined Higgs to tau-pair result includes a dedicted search using the associated production mechanism.

SM Higgs	Significance					
m_{H} [GeV]	-2σ	-1σ	Median	$+1\sigma$	$+2\sigma$	Observed
110	0.50	1.32	2.25	2.99	3.55	1.68
115	0.59	1.30	2.33	3.12	3.68	1.74
120	0.70	1.53	2.49	3.18	3.78	1.49
125	0.61	1.47	2.45	3.19	3.74	1.50
130	0.54	1.41	2.32	3.08	3.66	1.17
135	0.39	1.23	2.10	2.79	3.40	0.76
140	0.30	1.01	1.89	2.60	3.10	0.67
145	0.23	0.81	1.65	2.30	2.77	0.73

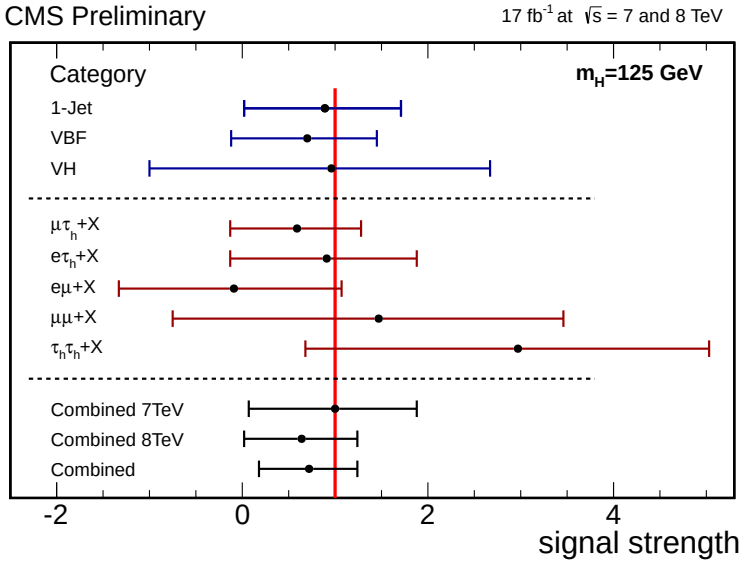

Figure 10: Best-fit signal strength values, $\sigma/\sigma_{\mathrm{SM\,H}}$, for various sub-combinations, ordered by production and decay mode, and the combination of the search channels. The red vertical line at one indicate the standard-model Higgs expectation.

$\mu\tau_h$+X, eτ_h+X, eμ+X, $\tau_h\tau_h$+X, and $\mu\mu$+X. The final result is combined with a Higgs search with tau pairs that uses the associated production of Higgs bosons with a W or Z boson decaying leptonically. Upper limits on the production cross section times that predicted by the standard model are determined, in the mass range 110-145 GeV, with observed (expected) 95% confidence level exclusion limits of 1.63 (1.00) for $m_{\mathrm{H}} = 125$ GeV.

References

[1] S. Weinberg, "A Model of Leptons", *Phys. Rev. Lett.* **19** (1967) 1264, doi:10.1103/PhysRevLett.19.1264.

[2] A. Salam, "Elementary Paricle Theory", p. 367. Almqvist and Wiksells, Stockholm, 1968.

[3] A. Salam, "Weak and electromagnetic interactions", in *Elementary particle physics: relativistic groups and analyticity*, N. Svartholm, ed., p. 367. Almqvist & Wiskell, Stockholm, 1968. Proceedings of the eighth Nobel symposium.

[4] F. Englert and R. Brout, "Broken symmetry and the mass of gauge vector mesons", *Phys. Rev. Lett.* **13** (1964) 321, doi:10.1103/PhysRevLett.13.321.

[5] P. W. Higgs, "Broken symmetries, massless particles and gauge fields", *Phys. Lett.* **12** (1964) 132, doi:10.1016/0031-9163(64)91136-9.

[6] P. W. Higgs, "Broken symmetries and the masses of gauge bosons", *Phys. Rev. Lett.* **13** (1964) 508, doi:10.1103/PhysRevLett.13.508.

[7] G. S. Guralnik, C. R. Hagen, and T. W. B. Kibble, "Global conservation laws and massless particles", *Phys. Rev. Lett.* **13** (1964) 585, doi:10.1103/PhysRevLett.13.585.

[8] P. W. Higgs, "Spontaneous symmetry breakdown without massless bosons", *Phys. Rev.* **145** (1966) 1156, doi:10.1103/PhysRev.145.1156.

[9] T. W. B. Kibble, "Symmetry breaking in non-Abelian gauge theories", *Phys. Rev.* **155** (1967) 1554, doi:10.1103/PhysRev.155.1554.

[10] ATLAS Collaboration Collaboration, "Observation of a new particle in the search for the Standard Model Higgs boson with the ATLAS detector at the LHC", *Phys.Lett.B* (2012) doi:10.1016/j.physletb.2012.08.020, arXiv:1207.7214.

[11] CMS Collaboration Collaboration, "Observation of a new boson at a mass of 125 GeV with the CMS experiment at the LHC", *Phys.Lett.B* (2012) doi:10.1016/j.physletb.2012.08.021, arXiv:1207.7235.

[12] CMS Collaboration, "The CMS experiment at the CERN LHC", *JINST* **3** (2008) S08004, doi:10.1088/1748-0221/3/08/S08004.

[13] CMS Collaboration, "Search for a standard model Higgs boson decaying to tau pairs produced in association with a W or Z boson", *CMS Physics Analysis Summary* **CMS-PAS-HIG-12-051** (2012).

[14] CMS Collaboration, "Particle–Flow Event Reconstruction in CMS and Performance for Jets, Taus, and $E_{\mathrm{T}}^{\mathrm{miss}}$", CMS Physics Analysis Summary CMS-PAS-PFT-09-001, (2009).

[15] CMS Collaboration, "Commissioning of the Particle-flow Event Reconstruction in Minimum-Bias and Jet Events from pp Collisions at 7 TeV", CMS Physics Analysis Summary CMS-PAS-PFT-10-002, (2010).

[16] CMS Collaboration, "Commissioning of the particle–flow event reconstruction with leptons from J/ψ and W decays at 7 TeV", CMS Physics Analysis Summary CMS-PAS-PFT-10-003, (2010).

[17] CMS Collaboration, "Determination of jet energy calibration and transverse momentum resolution in CMS", *JINST* **6** (2011) 11002, doi:10.1088/1748-0221/6/11/P11002, arXiv:1107.4277.

[18] M. Cacciari, G. P. Salam, and G. Soyez, "The anti-k_t jet clustering algorithm", *JHEP* **04** (2008) 063, doi:10.1088/1126-6708/2008/04/063, arXiv:0802.1189.

[19] M. Cacciari, G. P. Salam, "Dispelling the N^3 myth for the k_t jet-finder", *Phys. Lett. B* **641** (2006) 57, doi:10.1016/j.physletb.2006.08.037, arXiv:hep-ph/0512210.

[20] A. Hoecker et al., "TMVA - toolkit for multivariate data analysis", arXiv:0703039.

[21] CMS Collaboration, "Identification of b-quark jets with the CMS experiment", *CMS Physics Analysis Summary* **CMS-PAS-BTV-12-001** (2012).

[22] CMS Collaboration, "Performance of tau-lepton reconstruction and identification in CMS", *JINST* **7** (2012) P01001, doi:10.1088/1748-0221/7/01/P01001.

[23] CMS Collaboration, "Electron Reconstruction and Identification at $\sqrt{s} = 7$ TeV", CMS Physics Analysis Summary CMS-PAS-EGM-10-004, (2010).

[24] CMS Collaboration, "Performance of muon identification in pp collisions at $\sqrt{s}$ = 7 TeV", CMS Physics Analysis Summary CMS-PAS-MUO-10-002, (2010).

[25] CMS Collaboration, "Measurement of Inclusive Z Cross Section via Decays to Tau Pairs in pp Collisions at $\sqrt{s}$=7 TeV", *JHEP* **8** (2011) 117, doi:10.1007/JHEP08(2011)117.

[26] C. C. Almenar, "Search for the neutral MSSM Higgs bosons in the $\tau\tau$ decay channels at CDF Run II". PhD thesis, Universitat de València. FERMILAB-THESIS-2008-86. doi:10.2172/953708.

[27] R. K. Ellis, I. Hinchliffe, M. Soldate et al., "Higgs Decay to $\tau^+\tau^-$: A Possible Signature of Intermediate Mass Higgs Bosons at the SSC", *Nucl. Phys.* **B 297** (1988) 221.

[28] CMS Collaboration, "MET Performance in 2011 CMS Data", *CMS PAS* **DP-2012/003** (2012).

[29] CMS Collaboration, "MET Performance in 2012 Run A CMS Data", *CMS DP Note* **DP-2012/013** (2012).

[30] K. H. B. Bullok and A. Martin, "Tau polarization and its correlations as a probe of new physics", *Nucl. Phys.* **B** (1993) 395.

[31] CMS Collaboration Collaboration, "Missing transverse energy performance of the CMS detector", *JINST* **6** (2011) P09001, doi:10.1088/1748-0221/6/09/P09001, arXiv:1106.5048.

[32] J. Alwall, P. Demin, S. de Visscher et al., "MadGraph/MadEvent v4: the new web generation", *JHEP* **09** (2007) 028, doi:10.1088/1126-6708/2007/09/028, arXiv:0706.2334.

[33] T. Sjöstrand, S. Mrenna, and P. Skands, "PYTHIA 6.4 physics and manual", *JHEP* **05** (2006) 026, doi:10.1088/1126-6708/2006/05/026.

[34] P. Nason and C. Oleari, "NLO Higgs boson production via vector-boson fusion matched with shower in POWHEG", *JHEP* **02** (2010) 037, doi:10.1007/JHEP02(2010)037.

[35] S. Jadach, J. H. Kuhn, and Z. Wąs, "TAUOLA - a library of Monte Carlo programs to simulate decays of polarized tau leptons", *Computer Physics Communications* **64** (1991) 275, doi:10.1016/0010-4655(91)90038-M.

[36] C. Anastasiou, K. Melnikov, and F. Petriello, "Fully differential Higgs boson production and the di-photon signal through next-to-next-to-leading order", *Nucl. Phys. B* **724** (2005) 197, doi:10.1016/j.nuclphysb.2005.06.036.

[37] C. Anastasiou, S. Bucherer, and Z. Kunszt, "HPro: A NLO Monte-Carlo for Higgs production via gluon fusion with finite heavy quark masses", *JHEP* **10** (2009) 068, doi:10.1088/1126-6708/2009/10/068.

[38] CMS Collaboration, "Measurement of Inclusive W and Z Cross Sections in pp Collisions $\sqrt{s}$=7 TeV", *JHEP* **1110** (2011) 132, doi:10.1007/JHEP01(2011)080.

[39] CMS Collaboration, "Measurement of CMS Luminosity", CMS Physics Analysis Summary CMS-PAS-EWK-10-004, (2010).

[40] CMS Collaboration, "Performance of b-jet identification in CMS", CMS Physics Analysis Summary CMS-PAS-BTV-11-001, (2011).

[41] LHC Higgs Cross Section Working Group, S. Dittmaier, C. Mariotti et al., "Handbook of LHC Higgs Cross Sections: 1. Inclusive Observables", (CERN, Geneva, 2011). arXiv:1101.0593.

[42] A. Djouadi, M. Spira, and P. M. Zerwas, "Production of Higgs bosons in proton colliders: QCD corrections", *Phys. Lett. B* **264** (1991) 440, doi:10.1016/0370-2693(91)90375-Z.

[43] S. Dawson, "Radiative corrections to Higgs boson production", *Nucl. Phys. B* **359** (1991) 283, doi:10.1016/0550-3213(91)90061-2.

[44] M. Spira, A. Djouadi, D. Graudenz et al., "Higgs boson production at the LHC", *Nucl. Phys. B* **453** (1995) 17, doi:10.1016/0550-3213(95)00379-7, arXiv:hep-ph/9504378.

[45] R. V. Harlander and W. B. Kilgore, "Next-to-next-to-leading order Higgs production at hadron colliders", *Phys. Rev. Lett.* **88** (2002) 201801, doi:10.1103/PhysRevLett.88.201801, arXiv:hep-ph/0201206.

[46] C. Anastasiou and K. Melnikov, "Higgs boson production at hadron colliders in NNLO QCD", *Nucl. Phys. B* **646** (2002) 220, doi:10.1016/S0550-3213(02)00837-4, arXiv:hep-ph/0207004.

[47] V. Ravindran, J. Smith, and W. L. van Neerven, "NNLO corrections to the total cross section for Higgs boson production in hadron hadron collisions", *Nucl. Phys. B* **665** (2003) 325, doi:10.1016/S0550-3213(03)00457-7, arXiv:hep-ph/0302135.

[48] S. Catani, D. de Florian, M. Grazzini et al., "Soft-gluon resummation for Higgs boson production at hadron colliders", *JHEP* **07** (2003) 028, doi:10.1088/1126-6708/2003/07/028.

[49] U. Aglietti, R. Bonciani, G. Degrassi et al., "Two-loop light fermion contribution to Higgs production and decays", *Phys. Lett. B* **595** (2004) 432, doi:10.1016/j.physletb.2004.06.063, arXiv:hep-ph/0404071.

[50] G. Degrassi and F. Maltoni, "Two-loop electroweak corrections to Higgs production at hadron colliders", *Phys. Lett. B* **600** (2004) 255, doi:10.1016/j.physletb.2004.09.008, arXiv:hep-ph/0407249.

[51] S. Actis, G. Passarino, C. Sturm et al., "NLO Electroweak Corrections to Higgs Boson Production at Hadron Colliders", *Phys. Lett. B* **670** (2008) 12, doi:10.1016/j.physletb.2008.10.018, arXiv:0809.1301.

[52] C. Anastasiou, R. Boughezal, and F. Petriello, "Mixed QCD-electroweak corrections to Higgs boson production in gluon fusion", *JHEP* **04** (2009) 003, doi:10.1088/1126-6708/2009/04/003, arXiv:0811.3458.

[53] D. de Florian and M. Grazzini, "Higgs production through gluon fusion: updated cross sections at the Tevatron and the LHC", *Phys. Lett. B* **674** (2009) 291, doi:10.1016/j.physletb.2009.03.033, arXiv:0901.2427.

[54] J. Baglio and A. Djouadi, "Higgs production at the lHC", *JHEP* **03** (2011) 055, doi:10.1007/JHEP03(2011)055, arXiv:1012.0530.

[55] M. Ciccolini, A. Denner, and S. Dittmaier, "Strong and Electroweak Corrections to the Production of a Higgs Boson+2 Jets via Weak Interactions at the Large Hadron Collider", *Phys. Rev. Lett.* **99** (2007) 161803, doi:10.1103/PhysRevLett.99.161803, arXiv:0707.0381.

[56] M. Ciccolini, A. Denner, and S. Dittmaier, "Electroweak and QCD corrections to Higgs production via vector-boson fusion at the LHC", *Phys. Rev. D* **77** (2008) 013002, doi:10.1103/PhysRevD.77.013002, arXiv:0710.4749.

[57] K. Arnold, M. Bahr, G. Bozzi et al., "VBFNLO: A parton level Monte Carlo for processes with electroweak bosons", *Comput. Phys. Commun.* **180** (2009) 1661, doi:10.1016/j.cpc.2009.03.006, arXiv:0811.4559.

[58] O. Brein, A. Djouadi, and R. Harlander, "NNLO QCD corrections to the Higgs-strahlung processes at hadron colliders", *Phys. Lett. B* **579** (2004) 149, doi:10.1016/j.physletb.2003.10.112, arXiv:hep-ph/0307206.

[59] M. L. Ciccolini, S. Dittmaier, and M. Krämer, "Electroweak radiative corrections to associated WH and ZH production at hadron colliders", *Phys. Rev. D* **68** (2003) 073003, doi:10.1103/PhysRevD.68.073003, arXiv:hep-ph/0306234.

[60] A. Djouadi, J. Kalinowski, M. Muhlleitner et al., "An update of the program HDECAY", in *The Les Houches 2009 workshop on TeV colliders: The tools and Monte Carlo working group summary report*. 2010. arXiv:1003.1643.

[61] A. Denner, S. Heinemeyer, I. Puljak et al., "Standard Model Higgs-Boson Branching Ratios with Uncertainties", *Eur. Phys. J. C* **71** (2011) 1753, doi:10.1140/epjc/s10052-011-1753-8, arXiv:1107.5909.

[62] M. Botje et al., "The PDF4LHC Working Group Interim Recommendations", arXiv:1101.0538.

[63] S. Alekhin et al., "The PDF4LHC Working Group Interim Report", arXiv:1101.0536.

[64] H. Lai et al., "New parton distributions for collider physics", *Phys. Rev.* **D82** (2010) 074024, doi:10.1103/PhysRevD.82.074024, arXiv:1007.2241.

[65] NNPDF Collaboration, "Impact of Heavy Quark Masses on Parton Distributions and LHC Phenomenology", *Nucl. Phys. B* **849** (2011) 296, doi:10.1016/j.nuclphysb.2011.03.021, arXiv:1101.1300.

[66] J. S. Conway, "Nuisance Parameters in Likelihoods for Multisource Spectra", in *Proceedings of PHYSTAT 2011 Workshop on Statistical Issues Related to Discovery Claims in Search Experiments and Unfolding*, H. Propser and L. Lyons, eds., number CERN-2011-006, p. 115. CERN, 2011.

[67] T. Junk, "Confidence level computation for combining searches with small statistics", *Nucl. Instrum. Meth. A* **434** (1999) 435, doi:10.1016/S0168-9002(99)00498-2.

[68] A. L. Read, "Modified frequentist analysis of search results (the CLs method)", CERN Report CERN-OPEN-2000-005, (2000).

[69] ATLAS and CMS Collaborations, LHC Higgs Combination Group, "Procedure for the LHC Higgs boson search combination in Summer 2011", ATL-PHYS-PUB/CMS NOTE 2011-11, 2011/005, (2011).